



Earth's Future



RESEARCH ARTICLE

10.1029/2023EF003846

Key Points:

- 22 out of 27 cities show statistically significant downwind enhancement of climatological precipitation
- The precipitation patterns exhibit different spatial characteristics with varying meteorological conditions
- Downwind enhancement factor is positively correlated with city size under dominant wind direction

Supporting Information:

Supporting Information may be found in the online version of this article.

Correspondence to:

Q. Li, ql56@cornell.edu

Citation:

Lu, Y., Yu, Z., Albertson, J. D., Chen, H., Hu, L., Pendergrass, A., et al. (2024). Understanding the influence of urban form on the spatial pattern of precipitation. *Earth's Future*, 12, e2023EF003846. https://doi.org/10.1029/2023EF003846

Received 6 JUN 2023 Accepted 14 DEC 2023

© 2024 The Authors. This is an open access article under the terms of the Creative Commons Attribution-NonCommercial License, which permits use, distribution and reproduction in any medium, provided the original work is properly cited and is not used for commercial purposes.

Understanding the Influence of Urban Form on the Spatial Pattern of Precipitation

Yanle Lu¹, Zhou Yu¹, John D. Albertson¹, Haonan Chen², Leiqiu Hu³, Angeline Pendergrass⁴, Xiaodong Chen⁵, and Qi Li¹

¹School of Civil and Environmental Engineering, Cornell University, Ithaca, NY, USA, ²Department of Electrical and Computer Engineering, Colorado State University, Fort Collins, CO, USA, ³Department of Atmospheric and Earth Science, University of Alabama in Huntsville, Huntsville, AL, USA, ⁴Department of Earth and Atmospheric Science, Cornell University, Ithaca, NY, USA, ⁵Atmospheric Sciences and Global Change Division, Pacific Northwest National Laboratory, Richland, WA, USA

Abstract Urban areas are known to modify the spatial pattern of precipitation climatology. Existing observational evidence suggests that precipitation can be enhanced downwind of a city. Among the proposed mechanisms, the thermodynamic and aerodynamic processes in the urban lower atmosphere interact with the meteorological conditions and can play a key role in determining the resulting precipitation patterns. In addition, these processes are influenced by urban form, such as the impervious surface extent. This study aims to unravel how different urban forms impact the spatial patterns of precipitation climatology under different meteorological conditions. We use the Multi-Radar Multi-Sensor quantitative precipitation estimation data products and analyze the hourly precipitation maps for 27 selected cities across the continental United States from the years 2015-2021 summer months. Results show that about 80% of the studied cities exhibit a statistically significant downwind enhancement of precipitation. Additionally, we find that the precipitation pattern tends to be more spatially clustered in intensity under higher wind speed; the location of radial precipitation maxima is located closer to the city center under low background winds but shifts downwind under high wind conditions. The magnitude of downwind precipitation enhancement is highly dependent on wind directions and is positively correlated with the city size for the south, southwest, and west directions. This study presents observational evidence through a cross-city analysis that the urban precipitation pattern can be influenced by the urban modification of atmospheric processes, providing insight into the mechanistic link between future urban land-use change and hydroclimates.

Plain Language Summary Previous studies have shown that cities can influence the spatial rainfall patterns, and one of the strongest influences is that the precipitation tends to increase over downwind of city areas. The goal of this study is to understand how different urban forms impact rainfall spatial patterns under different weather conditions. We analyze the hourly precipitation accumulation data from Multi-Radar Multi-Sensor for a selected set of 25 cities across the continental United States from the years 2015–2021 summer months. The results indicate that more than 80% of the studied cities have a significant increase of rainfall in downwind regions. In addition, the rainfall spatial patterns have different characteristics with varying meteorological conditions such as precipitation intensities, wind speeds, and wind directions in terms of the location of rainfall maxima, the magnitude of downwind enhancement.

1. Introduction

Urbanization increased dramatically over the past few decades: 55% of the world's population residing in urban areas in 2018, and this trend is expected to keep increasing and reach 68% by 2050 (United Nations, 2018). Urbanization not only modifies land-use and land-cover and the resulting surface energy balance (Oke, 1982), but also has a notable impact on the patterns of temperature and precipitation (e.g., Freitag et al., 2018; Huff, 1975; Huff & Changnon, 1973; Zhou et al., 2017; Lorenz et al., 2019).

The so-called "urban rainfall effect" is clearly established in the literature: the majority of studies note an enhancement of rainfall in warm season convection (Bornstein & Lin, 2000; National Research Council, 2012; J. Shepherd et al., 2010); a recent meta-analysis across 85 quantitative studies conducted by J. Liu and Niyogi (2019) showed that cities affect precipitation and tend to increase over and/or downwind of urban areas, while studies vary regarding the magnitude and location of rainfall change, which is worthy of further investigation.

Possible mechanisms for urban areas to impact precipitation or hydrometeorology have been discussed through observation data and numerical modeling. The spatial contrasts in temperature and moisture induced by urban areas can modify precipitation through one or a combination of the following (J. M. Shepherd, 2005; Simón-Moral et al., 2021): First, the urban heat island (UHI) effect documented by many studies (e.g., Ganeshan et al., 2013; Santamouris, 2015) shows that the urban region can elevate local air temperature, increase sensible heat fluxes, cause corresponding destabilization of the boundary layer, and therefore, affect urban convection and precipitation. Second, the increased low-level wind convergence and bifurcation or diverting of precipitating convection systems due to increased surface roughness (e.g., Cotton & Pielke, 2007; Thielen et al., 2000). Third, the enhanced urban aerosol release can have contradictory effects on precipitation due to the modification of dynamical and microphysical processes in clouds (e.g., Andreae & Rosenfeld, 2008; Levin & Cotton, 2009; Schmid & Niyogi, 2017; Tao et al., 2007).

Actually, the large variability of urban-induced precipitation modification across the studies has been attributed to the fact that every city has its own unique layout and geographic background (Pathirana et al., 2014). The city-specific factors such as urban form (e.g., urban land surface characteristics, impervious surface fraction, city size, density of buildings, and orientation of street canyons) can influence the precipitation (e.g., Kellner & Niyogi, 2014; Kingfield et al., 2018) through the proposed mechanisms. For example, Miao et al. (2011) demonstrated that the degree of precipitation modification over Beijing has increased steadily with the growth of the city; W. Zhang et al. (2022) found that the circular city receives greater daily rainfall than the triangular city as the regional circulation is influenced by the city shapes, and such impact is more evident in the coastal environment. At the same time, the urban-induced rainfall changes are dependent on other factors. For example, results from previous studies underscore the importance of atmospheric flow regimes and background weather in affecting the precipitation anomaly for a given city (e.g., Shen & Yang, 2023; Yang et al., 2019, 2021).

Nevertheless, the interaction between meteorological factors and urban forms synergistically creates distinct urban atmospheric conditions, which complicates our understanding of individual controlling factors for urban modification on precipitation. Although numerical modeling by setting up controlled numerical experiments enables investigation of the effect of individual factors (e.g., Seino et al., 2018; Simón-Moral et al., 2021; Yang et al., 2019) for a given city, generalization across multiple cities is difficult. On the other hand, observational studies on urban precipitation can potentially help with generalization across distinct cities, yet the effect of individual controlling factors can hardly be separated and inferring the urban effect on precipitation remains challenging. The majority of individual studies are single-city-based, event-based, or focusing on one type of precipitation event, such as thunderstorms (e.g., Dou et al., 2015; Lorenz et al., 2019). As a result, various findings have been reported in different studies with diverse conclusions regarding the impact of cities on precipitation. Those analyses/case studies can introduce implicit bias when they are considered representative to generalize the results (J. Liu & Niyogi, 2019). Furthermore, as urban land use and land cover change continues, an improved understanding of how cities modify the climatological precipitation pattern is important to guide future urban development.

Therefore, we seek to investigate the urban modification of rainfall events by going beyond analyzing individual cities under certain regional climate conditions, so as to generalize the urban impacts on the spatial pattern of precipitation and the underlying causes across a broad range of urban forms. To address our research goal, we conduct a cross-city analysis with selected 27 cities across the continental United States considering a broad spectrum of urban forms and regional climate contexts. We only focus on climatological performance across cities but not the difference between individual cities. We deliberately choose not to track the development of a single event, so as to avoid analyzing the simultaneous interactions between multiple factors that are event-dependent. Summer precipitation for 6 years (2015–2021) is considered. In addition, we start by investigating the downwind enhancement of precipitation in this study as it is one of the strongest influences reported by previous studies (e.g., Han et al., 2014; J. Liu & Niyogi, 2019; Shem & Shepherd, 2009), while most of them are case studies or single-city-based studies. Section 2 introduces the data set and the metrics we use to analyze and quantify the downwind enhancement and other spatial anomalies. The results and corresponding analysis are included in Section 3. Section 4 is the discussion and conclusion.

2. Data and Methods

2.1. Multi-Radar Multi-Sensor (MRMS) Quantitative Precipitation Estimation (QPE) Data

Multi-Radar Multi-Sensor (MRMS) data set is a publicly available data set deployed operationally in 2014 at the National Center for Environmental Prediction (NCEP). The MRMS system incorporates fully automated

LU ET AL. 2 of 15

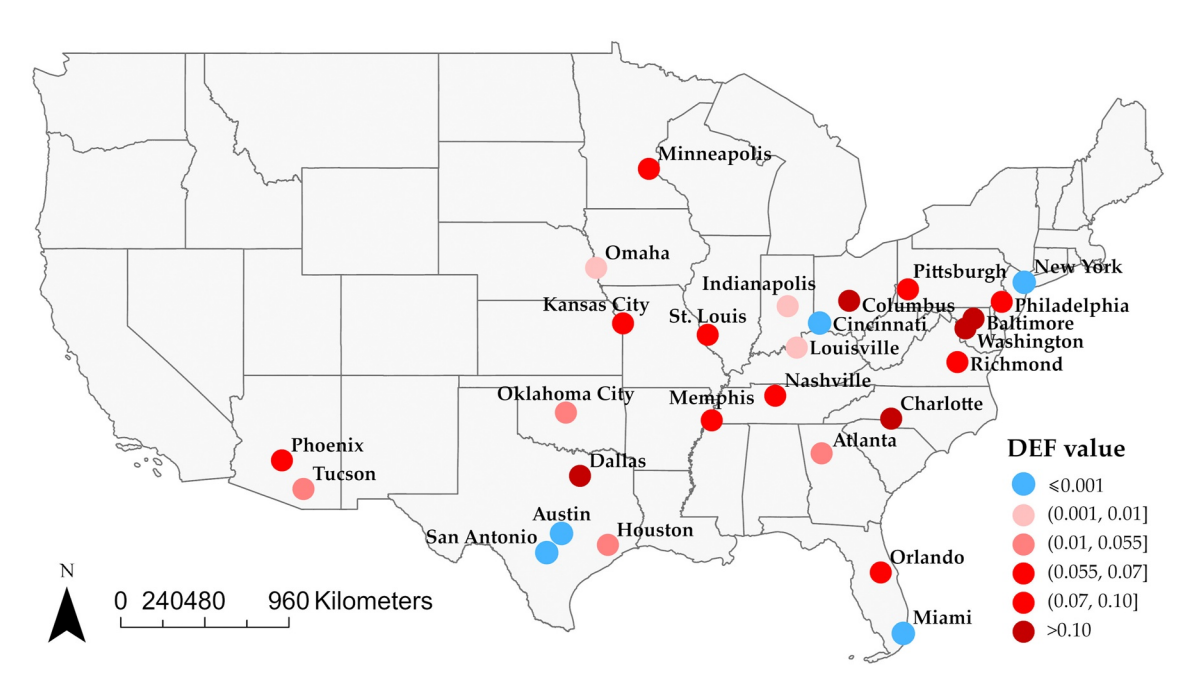


Figure 1. Study areas of selected 25 cities for this study plus 2 coastal cities (i.e., Miami and New York City) for comparison. The color refers to their corresponding climatological downwind enhancement factor (DEF) value. The red color indicates the city has statistically significant downwind enhancement for climatological precipitation spatial pattern; the blue color indicates the city has a negative DEF value (i.e., New York, Austin, San Antonio, and Miami) or a statistically insignificant positive DEF value (i.e., Cincinnati). See Section 3.1 for more details.

algorithms that quickly and intelligently integrate data streams from multiple radars, surface and upper air observations, lightning detection systems, satellite observations, rain gauge observations and forecasted models. It then creates a seamless 3D mosaic across the conterminous United States (CONUS) and southern Canada at very high spatial (1 km) and temporal (2 min) resolution, and includes more than one hundred products offering assistance for quantitative precipitation estimation (QPE), turbulence diagnosis, etc. (More details at: https://www.nssl.noaa.gov/projects/mrms/).

The Multi-radar integration can mitigate the deficiencies in the single-radar framework. The integration of radar with multi-sensor data can provide more accurate diagnoses of physical processes in the atmosphere. Such an integration process provides enhanced QPE products (J. Zhang et al., 2016). In addition, the radar data quality control algorithms undergo continuous refinements to effectively identify and remove various non-hydrometeor radar echoes and ensure QPE products have robust performance across seasons and all regions (Tang et al., 2020).

MRMS data is hence widely used to analyze precipitation spatial patterns as it allows for detailed and accurate quantification of precipitation at a high spatial and temporal resolution (e.g., Lengfeld et al., 2020; Sungmin & Kirstetter, 2018). This also makes it ideal for studying the spatial pattern of precipitation in urban areas. Therefore, in this study, we use the MRMS QPE product of hourly precipitation accumulation for 25 cities across the continental United States plus 2 coastal cities (i.e., Miami and New York City) from the years 2015–2021 summer months (i.e., June, July, and August), spanning 15456 hr in total.

Only two coastal cities, Miami and New York City are included in climatological analysis among other inland cities for comparison, which are expected to be more complex involving strong local land-sea breeze circulation as the study areas include some ocean area. In addition, west coast cities and mountain region cities are excluded due to the small amount of summer rain and the influence of topography. For each city, the research domain is defined as a 60 km circular area with the city located at the center of the circle, which is characterized by 100% of impervious land use type. The size of the study areas is decided by previous studies that the influence of the urban structures mainly appears within 50–60 km. For example, Lorenz et al. (2019) found evidence of urban rainfall intensification about 20–50 km downwind of the urban center; J. Liu and Niyogi (2019) found the distance of precipitation modification is 26–52 km around the cities with a meta-analysis across case studies, climatology studies, and modeling studies. The selected cities and corresponding research domains are shown in Figure 1.

LU ET AL. 3 of 15

2.2. Modern-Era Retrospective Analysis for Research and Applications, Version 2 (MERRA-2)

The Modern-Era Retrospective analysis for Research and Applications, Version 2 (MERRA-2) is the latest version of global atmospheric reanalysis for the satellite era produced by NASA Global Modeling and Assimilation Office (GMAO) using the upgraded version 5.12.4 of Goddard Earth Observing System Model (GEOS) (Gelaro et al., 2017). The data set covers the period of 1980—present. It was introduced because of the advances made in both the GEOS model and the assimilation system that enable the assimilation of modern hyperspectral radiance and microwave observations, along with GPS-Radio Occultation data sets. McCarty et al. (2016) describe the input observations for the MERRA-2 data assimilation process, and more details about MERRA-2 can be found at https://gmao.gsfc.nasa.gov/reanalysis/MERRA-2/docs/.

These global reanalysis data have the advantage of providing globally consistent information that can provide detailed information on wind patterns across a large area, including CONUS. The MERRA-2 grid has an approximate resolution of $0.5^{\circ} \times 0.625^{\circ}$ in latitude and longitude (known as native resolution), corresponding to a spatial resolution of approximately 50 km in the latitudinal direction.

In this study, we use the M2T1NXSLV (or tavg1_2d_slv_Nx) data collection, which corresponds to hourly time-averaged two-dimensional data consisting of meteorology diagnostics at popularly used vertical levels (Global Modeling and Assimilation Office & Pawson, 2015). Compared with the 500 hPa data which determine large-scale conditions, the 850 hPa circulation conditions can more clearly display the specific weather processes (Y.-Y. Liu et al., 2021) and thus can provide information about the movement of weather systems. In addition, the 850 hPa represents the top (or close to the top) of the planetary boundary layer for the locations close to sea level, which can reflect the surface impacts while having a more stable value. Therefore, the wind components at 850 hPa are used as the background wind for analysis, and the same time period as the precipitation data set, years 2015–2021 summer months, is selected.

2.3. Moderate Resolution Imaging Spectroradiometer (MODIS) Land Cover Type Product and City Size

The Terra and Aqua combined Moderate Resolution Imaging Spectroradiometer (MODIS) Land Cover Type (MCD12Q1) Version 6 data product is used to identify the urban areas and calculate the imperviousness profile used in Section 3.4.

The MCD12Q1 data set provides global land cover types at yearly intervals 2001–2020 with the spatial resolution as 500 m, derived using the supervised decision-tree classification method with MODIS Terra and Aqua reflectance data (Friedl et al., 2002, 2010) and additional post-processing that incorporates prior knowledge and ancillary information to further refine specific classes. It consists of six different classification schemes, and the Annual University of Maryland (UMD) classification (Hansen et al., 2000) is used in this study. More details about this data set can be found at https://lpdaac.usgs.gov/products/mcd12q1v006/.

The urban and built-up lands defined in UMD classification is at least 30% impervious surface area including building materials, asphalt, and vehicles. In this study, the pixels identified as urban and built-up lands are considered as impervious areas, and other types are considered as non-urban areas. Then the percentage of impervious areas can be calculated using the number of pixels occupied by the urban and built-up lands divided by the total number of pixels.

The imperviousness is commonly associated with urbanization level and the spatial variation of imperviousness around the city center is a characteristic of urban forms. Specifically, the imperviousness profile, which is defined as the percentage value from the city center to the edge of the study area along eight absolute directions (east (E), north-east (NE), north (N), north-west (NW), west (W), south-west (SW), south (S) and south-east (SE)), offers a reduced dimensional representation of the two-dimensional (2D) urban form at the local scale. Each direction contains pixels in the corresponding circular sector of 45° and the percentage value is calculated for each 3 km along the direction. The impervious ratio near the city center is around one and decreases from the city center to the edge. The shapes of the imperviousness profile are expected to be different for each direction as most cities are not symmetric. The city size is estimated based on imperviousness greater than 0.5 and is conditioned on the direction. The schematic of the definition of city size using the imperviousness profile is shown in Figure 2a.

LU ET AL. 4 of 15

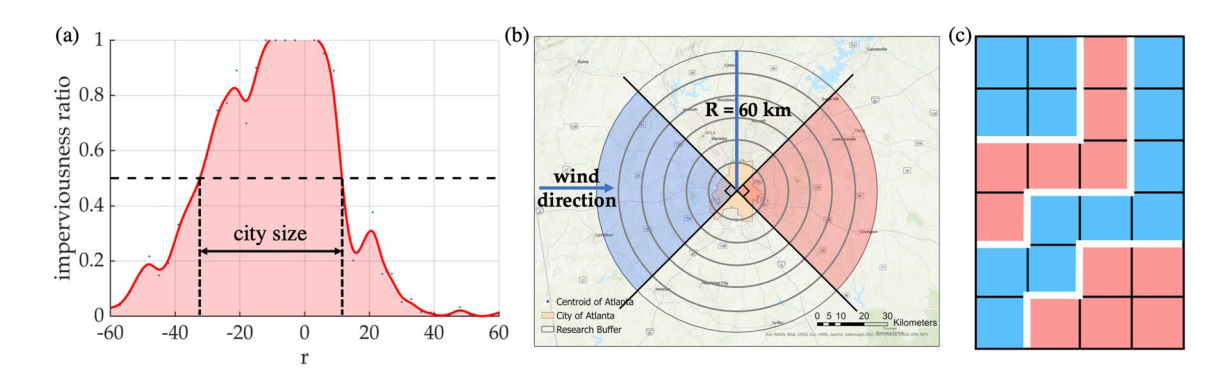


Figure 2. (a) The imperviousness profile where r denotes distance from city center from upwind to downwind direction. Dashed vertical lines define the city size; (b) The definition of upwind and downwind regions, and the schematic of the radial profile $\Phi(r)$ of precipitation averaged over upwind and downwind quadrants (cf., Section 2.4.4). The blue-shaded region is the upwind region (A_{up}) , and the red-shaded region is the downwind region (A_{down}) ; (c) The schematic of the length of zero line (LZL, cf., Section 2.4.3), which is indicated by the white line.

2.4. Quantitative Metrics for Precipitation Spatial Patterns

There is no standard method to objectively identify the modifications of precipitation patterns by urban areas (Lorenz et al., 2019). In this study, we consider the following metrics to quantify precipitation modification induced by urban areas from different perspectives.

2.4.1. Downwind Enhancement Factor (DEF)

The MRMS hourly precipitation data is first pre-processed by rotating each hourly precipitation data of each city based on the corresponding wind direction so that the wind is coming from the same direction, that is, here taken as from left, as indicated by Figure 2b. This allows the upwind region and downwind quadrants from different hours to be superimposed to better isolate the urban signals and be standardized for later comparison. We use $\widetilde{p}(\vec{x},t)$ to represent the rotated MRMS precipitation data at a specific hour t at location \vec{x} . The symbol $p(\vec{x})$ represents the pixel-wise summation of $\widetilde{p}(\vec{x},t)$ over some specific condition, that is, some subset T_{cond} of all hours in the study period T based on the specific conditions. It is defined as:

$$p(\vec{x}) = \frac{\sum_{t} \widetilde{p}(\vec{x}, t) I(t)}{\sum_{t} I(t)}, I(t) = \begin{cases} 0 & t \notin T_{cond} \\ 1 & t \in T_{cond} \end{cases}$$
(1)

The downwind enhancement factor (DEF) is then defined using $p(\vec{x})$ to evaluate the precipitation difference between the upwind and downwind regions of a city and quantify the magnitude of the downwind enhancement of precipitation. It is calculated using the precipitation summed over the upwind region $(\int_{A_{up}} p \, da)$ and downwind region $(\int_{A_{down}} p \, da)$ following Equation 2. The upwind and downwind regions are quadrant shapes defined with wind direction. The example of the upwind region, downwind region, and their relationship with wind direction is shown in Figure 2b.

$$DEF = \frac{\int_{A_{down}} p \, \mathrm{d}a - \int_{A_{up}} p \, \mathrm{d}a}{\int_{A_{down}} p \, \mathrm{d}a + \int_{A_{up}} p \, \mathrm{d}a},\tag{2}$$

where A_{down} and A_{up} represent the downwind region and upwind region, $\int_{A_{down}} p \, da$ and $\int_{A_{up}} p \, da$ represent the sum of precipitation over the downwind and upwind regions in a given time period, respectively. With this definition, DEF is a number between [-1,1]. If it is larger than 0, it means that the downwind enhancement of precipitation does exist, and the larger the value, the higher the downwind enhancement.

LU ET AL. 5 of 15

2.4.2. Normalized Spatial Distribution

Normalizing the spatial distribution enables us to better investigate the spatial patterns within and among the study areas and to make comparisons on a common scale without being influenced by the absolute amount of climatological precipitation across cities. The normalization is calculated using the following equation:

$$p^*(\vec{x}) = \frac{p(\vec{x}) - P}{\sigma},$$

$$P = \frac{\int_A p \, da}{A}, \sigma^2 = \frac{\int_A (p - P)^2 \, da}{A}$$
(3)

where $p^*(\vec{x})$ is the normalized precipitation, $p(\vec{x})$ is the value in the spatial distribution of precipitation summed up over a specific time range or some conditions; P and σ are the spatial mean value and the standard deviation of $p(\vec{x})$ in the 60km-radius study area A, respectively. There is no special treatment for pixels with zero value. One example of the normalized spatial distribution conditioned on different wind speeds for Dallas is shown in Figure S5 in Supporting Information S1. More details of the conditionally averaged normalized precipitation will be discussed in Section 3.

2.4.3. Length of Zero Line (LZL)

The length of zero line (LZL) is a metric defined to quantitatively evaluate the spatial pattern of precipitation. Specifically, it is calculated by counting the total number of grids on the normalized precipitation distribution $p^*(\vec{x})$ where it changes signs from its neighboring grid. That is, one is added to the LZL once any sign-changing between neighbors is observed.

The schematic of LZL is shown in Figure 2c, where the zero line is indicated by the white color. A larger LZL value indicates that there are more grids that have different signs with their neighbors, and therefore means the spatial pattern is more scattered. On the other hand, a smaller LZL value means that the spatial pattern is more clustered.

This metric is useful for understanding the spatial coherence of precipitation patterns. It is important to note that the LZL is only suitable for the normalized spatial distribution of precipitation. More details and explanations using this metric can be referred to in Sections 3.2 and 3.3.

2.4.4. Radial Profile $(\Phi(r))$ of Precipitation

The location of the radial precipitation maximum relative to the city center is an important indicator of spatial patterns and is evaluated by the radial profile $\Phi(r)$ averaged over upwind and downwind quadrants of precipitation.

 $\Phi(r)$ is obtained from the mean value of the quarter ring of precipitation distribution along the radius of the upwind and downwind directions. Specifically, the mean value is calculated for the quarter ring of each 10 km in the blue-shaded (upwind) and red-shaded (downwind) regions as shown in Figure 2b. These values are then used to get the radial profile $\Phi(r)$.

The radial profile $\Phi(r)$ illustrates the relative intensity of precipitation along the radius and helps identify the trends, such as whether the precipitation is more intense at the center or at the edges. $\Phi(r)$ can be obtained by either the original precipitation distribution $p(\vec{x})$ or the normalized precipitation distribution $p^*(\vec{x})$. The $\Phi(r)$ calculated using $p(\vec{x})$ is better at indicating the variation of absolute magnitudes of precipitation, while $p^*(\vec{x})$ is used to highlight differences in trends across different conditions. The advantage of this metric lies in its ability to extract effective information from a high-dimensional 2D map while conveying more information than a DEF value.

In addition, the average of radial profiles $\Phi(r)$ across all the cities is also calculated in the following sections, as the characteristics of the profiles for each city may be influenced by multiple factors other than the urban form and meteorological conditions explicitly considered here. This serves to average out the effects of other factors on the spatial distribution of precipitation, which are unaccounted for in the analysis, such as the magnitude of surface urban heat island and pre-storm environments Dou et al. (2015) and Shen and Yang (2023). Thus, the average of $\Phi(r)$ across all the cities is useful to understand the overall trend due to the interaction between urban structures and specific meteorological conditions.

LU ET AL. 6 of 15

3. Results and Discussion

The precipitation distribution can be influenced by many city-specific factors for each individual city. Therefore, the results of individual cities are expected to differ for precipitation spatial patterns. This study does not intend to explain all the differences among cities. Instead, the goal is to understand the synergistic effect of background regional conditions and urban forms across different cities, with a special focus on the downwind and upwind precipitation differences.

3.1. Climatological Precipitation Spatial Pattern

To investigate if downwind enhancement is a widely observed phenomenon induced by urban areas, we first evaluate the climatological precipitation for summer months over 6 years for the selected 25 cities plus Miami and New York City.

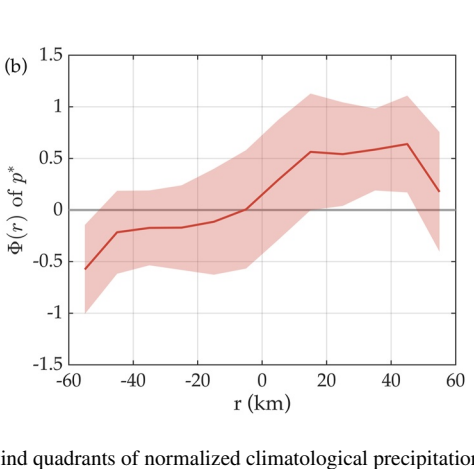
All the precipitating hours from the hourly data of precipitation for the study areas over the study period are selected to represent the climatological distribution. Here the precipitating hours are the hours that the mean precipitation accumulation is larger or equal to 0.1 mm. Three metrics conveying information from a number, one-dimension (1D) profile, and two-dimensional (2D) spatial distribution are considered to evaluate the downwind enhancement of precipitation among cities. Specifically, the DEF value, the radial profile $\Phi(r)$, and the normalized spatial distribution $p^*(\vec{x})$ are considered.

The climatological precipitation distribution $p(\vec{x})$ for each city is composited of all hourly MRMS precipitation data aligned based on the corresponding wind direction $\tilde{p}(\vec{x},t)$ over precipitating hours. The climatological DEF for each city is then calculated based on this climatological distribution using Equation 2 defined in Section 2.4.1. The DEF values vary across cities with the mean value of 0.050, the interquartile range of 0.079, and the standard deviation of 0.056. The t-test with a significance level of 0.05 is then applied to test for the presence of downwind enhancement of precipitation, that is, whether the spatial mean of the precipitation over the downwind region is significantly larger than that of the upwind region. The magnitude of DEF for each city is indicated in Figure 1 with colors. The darker the red color means the larger the climatology DEF value and the more significant the downwind enhancement of precipitation. The results show that more than four-fifths of all the study areas, that is, 22 cities, have significant positive DEF except for four cities (Austin, Miami, New York City, and San Antonio) with negative DEF and one city (Cincinnati) with an insignificant positive DEF. These cities might have other distinct climatological precipitation patterns caused by factors distinct from the rest. For example, as expected, Miami and New York City are both coastal cities with unusual city shapes, which are expected to have a strong sea breeze circulation influence; San Antonio and Austin are influenced by the natural gradient induced by the Edward Plateau and the Gulf of Mexico. Such performance is also reported in previous studies. For example, J. M. Shepherd et al. (2002) analyzed rainfall modification by major urban areas using data from the Tropical Rainfall Measuring Mission (TRMM) satellite and found only San Antonio has a negative value of downwind enhancement out of five studied cities. The climatological DEF results indicate that precipitation enhancement downwind of cities is a widely existing phenomenon.

The normalized climatological precipitation distribution is further examined following the methodology described in Section 2.4.2, and the results can be referred to in Figure S1 in Supporting Information S1. The objective is to better recognize and compare the characteristics of spatial anomalies across multiple cities. The dashed black lines are auxiliary lines that assist in distinguishing the upwind (left) and downwind (right) regions. The results indicate that a majority of cities exhibit an abundance of negative values (blue areas) in the upwind region, signifying lower precipitation intensity relative to the mean value, while the downwind region predominantly exhibits positive values (red areas). We also notice that not all the positive anomalies appear at the downwind quadrant. For example, the phenomenon of lateral enhancement of precipitation is observed in some cities such as Houston and Louisville, which is also reported mentioned by J. Liu and Niyogi (2019). This intriguing phenomenon is beyond the scope of this study and is worth further investigation in future studies.

The radial profile $\Phi(r)$ for climatological precipitation of each city is calculated using the normalized distribution following the definition in Section 2.4.4 to investigate the mean precipitation along the radius of the upwind and downwind direction. The individual profiles for each city are shown in Figure 3a, and the averaged profile across all cities, along with standard deviation, is shown in Figure 3b. The results show the consistency of the trend among all the study areas and indicate the center of the precipitation is located approximately 20–40 km

LU ET AL. 7 of 15



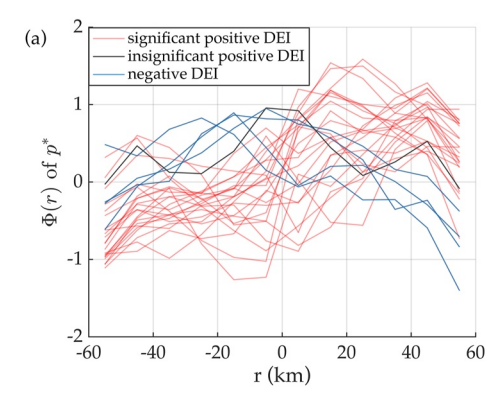


Figure 3. Radial profiles $\Phi(r)$ averaged over upwind and downwind quadrants of normalized climatological precipitation distribution p^* for (a) each city, and (b) the mean profile of all cities with standard deviation across cities. The negative ticks for the *x*-axis mean the upwind region and the positive ticks mean the downwind region.

downwind direction from the city center, which is consistent with previous studies (e.g., J. Liu & Niyogi, 2019; Lorenz et al., 2019).

It can be concluded from all three metrics considered here that downwind enhancement of precipitation climatology is a common characteristic across majority of the studied cities. In the following sections, we will focus on the 25 cities, excluding Miami and New York City, to investigate how the urban form and meteorological conditions influence the precipitation spatial pattern if significant downwind enhancement exists. These cities will be referred to as selected cities. All the precipitating hours will be classified according to different meteorological conditions and local factors pertaining to the urban form to further understand how the city modifies the rainfall patterns. Specifically, the mesoscale meteorological factors such as total precipitation, wind speed, and wind direction, and the local factors such as the imperviousness trend and city size are considered.

3.2. Variation of Precipitation Spatial Pattern With Intensity

The spatial distribution of precipitation with varying intensities is first analyzed, as the total amount of precipitation in the study area can be an important indicator of meteorological conditions. For each decile, all the hourly precipitation distributions are rotated to superimpose the upwind and downwind regions and obtain the precipitation distribution, similar to the climatological analysis above.

The shape of the probability distribution of precipitation intensity shows consistency across all the study areas and roughly follows an exponential distribution for all cities (see Figure S2 in Supporting Information S1). The low-intensity precipitation occurs more frequently, with a larger probability, and the probability decreases exponentially as the intensity increases. The deciles of precipitation intensity are considered to analyze the trend, and the exact values of deciles can be referred to in Table S1 in Supporting Information S1.

The normalized precipitation distributions of each decile demonstrate some consistency across the cities. For lower precipitation intensity, the spatial pattern is more scattered, and the large values tend to appear outside of the city center, while the small values appear in the city center. Scattering means that the positive areas and negative areas tend to be more randomly distributed in the study area, while clustering means that the positive areas and negative areas are gathered together. The length of zero line (LZL) of the normalized precipitation distribution is calculated over study areas to assess the observed spatial patterns based on the definition in Section 2.4.3. If the normalized distribution is more scattered, it will have more grids that have different signs with their neighbors, resulting in a larger LZL value. The box plot of the LZL for all the cities is shown in Figure 4a. The trend indicates that the values of LZL are similar for the first four deciles, with similar mean values and slightly changed standard deviations; then the values gradually decrease as the intensity increases and have a sharp drop between the 9th and 10th decile.

The radial profile $\Phi(r)$ of normalized precipitation distribution p^* is evaluated to further extract the spatial characteristics. The results show that the profiles exhibit a relatively consistent pattern across the cities (see Figure S3 in Supporting Information S1). For light precipitation, the precipitation intensity tends to be smaller near the

LU ET AL. 8 of 15

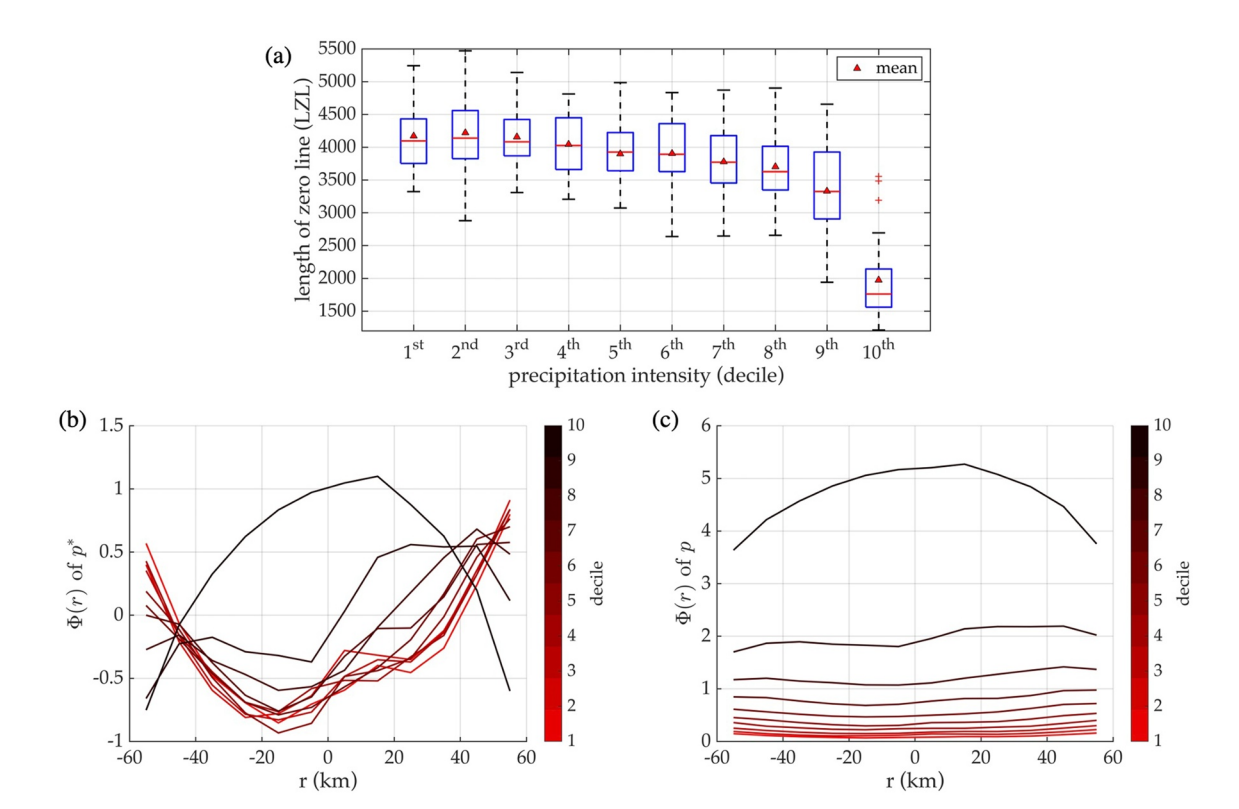


Figure 4. (a) LZL for all cities across deciles of precipitation intensity; (b) averaged radial profile $\Phi(r)$ across cities of precipitation distribution p, and (c) normalized precipitation distribution p^* . Lines in (b) and (c) represent deciles of precipitation intensity as indicated by the colorbar. On each box in (a), the central mark indicates the median, the bottom and top edges of the box indicate the 25th and 75th percentiles, respectively, the whiskers extend to the most extreme data points are considered outliers, and the outliers are plotted individually using the "+" marker symbol.

city center, and larger around the city, while the absolute difference is small. However, for heavy precipitation, the trend is the opposite, especially for the 10th decile indicated by the black line in Figure 4. It shows a clear difference of the 10th and 9th deciles compared to other deciles, while the absolute difference is now large and the average performance of all hours is dominated by the 10th and 9th deciles to some extent. In addition, there is a transition between the 1st and 10th decile that the relative precipitation center tends to move from the city edge toward the city center in the downwind region.

In summary, the spatial pattern of precipitation under different precipitation intensities does show consistency across the selected cities. For higher-intensity precipitation hours, the spatial anomalies of precipitation are more clustered and the radial profile indicates that the maxima of $\Phi(r)$ shifts toward the city center. These findings imply that urban areas show different effects among various precipitation intensities, and further research with more detailed data can be conducted to elucidate this relationship.

3.3. Variation of Precipitation Spatial Pattern With Wind Speed

The wind speed is divided into four quartiles based on the values for each city. For each quartile, the same procedure is applied to get the precipitation distribution, and then calculate the corresponding DEF values using Equation 2. Normalization is applied following Equation 3 to get the normalized precipitation distribution.

The values of DEF do not have a clear trend with different wind speeds (see Figure S4 in Supporting Information S1). However, the spatial clustering patterns of normalized precipitation distribution indicate that spatial anomalies vary with wind speeds. Two example cities (Dallas and Tuscon) are included in Supporting Information S1 (Figure S5) for reference, where the normalized precipitation distribution tends to be more clustered at high wind speed and scattered at low wind speed. To demonstrate that such a generalizable trend across cities, the length of zero line (LZL) of the normalized spatial distribution is calculated based on the definition in Section 2.4.3. The box plot of the LZL for all the cities is shown in Figure 5, indicating a clear trend that with higher wind speed, the LZL is shorter, and therefore the spatial pattern is more clustered.

LU ET AL. 9 of 15



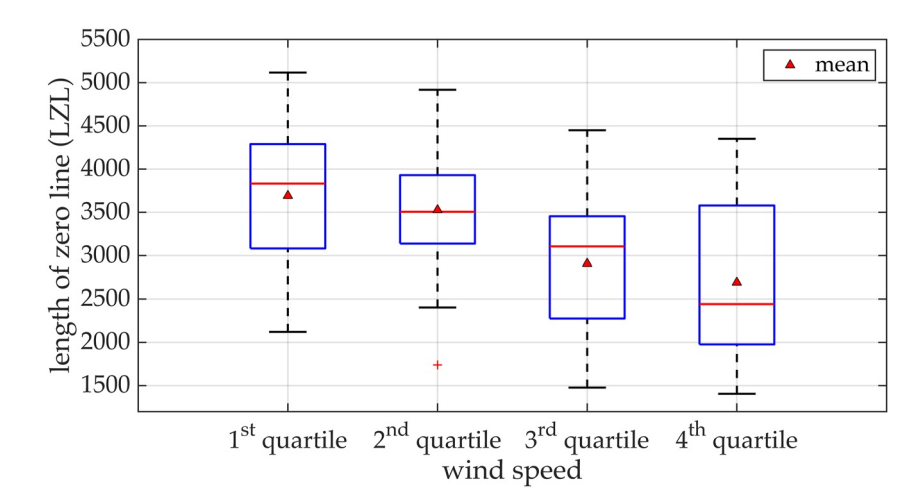


Figure 5. The box plot of LZL for all the cities under different wind speeds.

Location of the peak of $\Phi(r)$ with respect to the city center, that is, r = 0, is also an important indicator of the precipitation spatial patterns. The radial profile $\Phi(r)$ is defined in Section 2.4.4. The averaged profile across all cities for non-normalized and normalized precipitation distribution are shown in Figure 6 for understanding the influence introduced by wind speed and its interaction with urban structures.

Figure 6a indicates that the precipitation intensity is positively correlated with wind speed. The higher wind speed corresponds to larger mean precipitation in the study areas. The location for precipitation maxima is located closer to the city center under low background wind speed but shifts toward more downwind under high wind conditions as shown in Figure 6b. It can be speculated that the mixed-convective motions around a city are determined by the interactions between local urban-rural circulation and background wind. These flow interactions can be categorized into different regimes ranging from advection-dominated (plume regime) to convection-driven (bubble regime) (Omidvar et al., 2020). The urban-rural circulation induced by the urban heat island (UHI) phenomenon dominates under lower regional wind speeds and exhibits a circulation pattern with strong upward air motion at the city center. That is, the atmospheric boundary layer is more unstable near the city center with an intense uplifting of air. Therefore, precipitation tends to occur over the city center. However, under higher wind speeds, the UHI intensity is smaller compared to low wind speeds (e.g., Dou et al., 2015; Ngarambe et al., 2021; Shen & Yang, 2023) reported by multiple studies and the urban-rural circulation is weaker. The background wind dominates the flow pattern around the city, which corresponds to the plume regime. The convergence of air induced mainly by the surface roughness results in not only upward motions but also a downwind advective transport. These findings corroborate with the existing postulation about the urban thermal and roughness effects on precipitation. In addition, in light of the preferential deposition of precipitation given a steep topography (Lehning et al., 2008), it could be hypothesized that presence of urban structures modifies the downfall dynamics of the

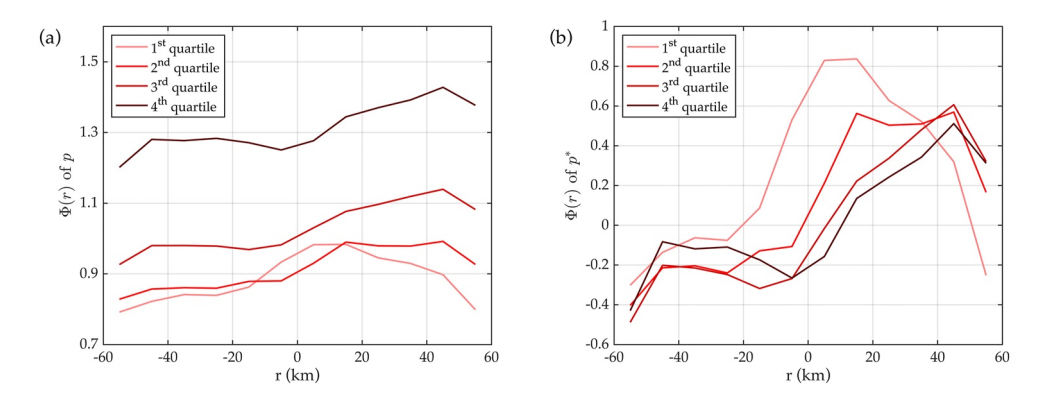


Figure 6. Radial profile $\Phi(r)$ of (a) precipitation distribution p, and (b) normalized precipitation distribution p^* under different wind speeds.

LU ET AL. 10 of 15



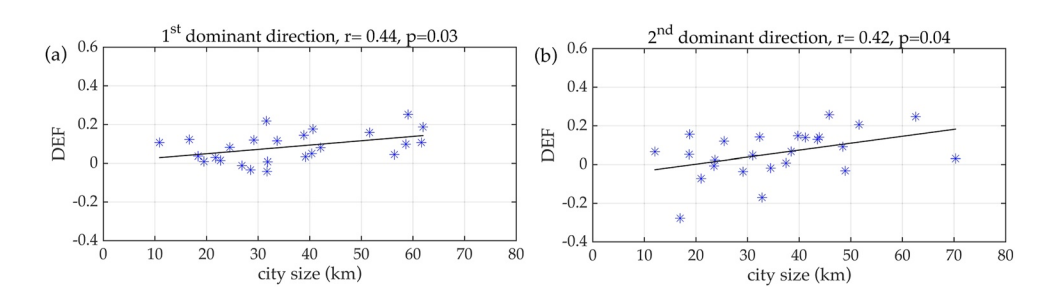


Figure 7. DEF versus city size for (a) first and (b) second dominant wind directions.

precipitation. Thus, if the precipitation forms over the center of the city, it can be transported downwind before its deposition. It can be stipulated that a similar mechanism occurs and the maximum precipitation moves further downwind of the city center compared to lower wind speeds. Although empirical evidence here does not allow one to precisely study this process, future research with numerical simulations will be able to better examine spatial patterns in both the droplet formation and deposition processes.

In summary, while the DEF values do not show a clear trend with background wind speed, the interaction between urban structures and different wind speeds changes, resulting in different spatial patterns of precipitation. The location for precipitation maximum tends to be closer to the city center, and the spatial distribution tends to be more scattered for lower wind speeds.

3.4. Variation of Precipitation Spatial Pattern With Wind Directions

The influence of wind direction is investigated in this section by dividing all the precipitating hours into eight absolute wind directions: east (E), north-east (NE), north (N), north-west (NW), west (W), south-west (SW), south (S), and south-east (SE). The same methodology is applied and the DEF values for each wind direction are calculated. The DEF values and the point plot and box plot of DEF values can be referred to in Supporting Information S1 (Figure S6 and Figure S7). They both indicate that the magnitude of DEF values is changing with the wind direction. There are more negative DEF values for E, SE, and NE directions, while the values are almost all positive for NW, W, and SW directions.

To further understand the overall trend of wind direction-dependent values of DEF across different cities, we consider the dominant wind direction since it corresponds to the dominant climatology circulation pattern. Specifically, the study areas in this study are influenced by the westerlies (Booth et al., 2006) and Bermuda high over the Atlantic Ocean and for the most area among CONUS in summer (Katz et al., 2003; Li et al., 2011). The wind rose (see Figure S8 in Supporting Information S1) for precipitating hours shows consistency of the first two dominant wind directions across cities: most of the cities have west (W) and southwest (SW) as the first two dominant wind directions, while six cities (e.g., Omaha, Oklahoma City, Dallas, San Antonio, Houston, and Austin) have south (S) wind. Only San Antonio and Houston have southeast (SE), and Austin has east (E) as the second dominant wind direction. They are all in the state of Texas and the dominant wind directions are highly influenced by the Gulf Coast.

The local factors such as urban roughness are known to influence the spatial distribution of precipitation. The imperviousness of land surface is commonly associated with urbanization level and can be considered as an indicator of urban roughness. Then we defined city size, one characteristic of the urban form, by considering the wind-direction-dependent imperviousness profile (cf. Section 2.3).

The first and second dominant wind directions for each city are first considered to establish the relationship between DEF value and city size. The scatter plot and corresponding linear regression are shown in Figure 7 with regression coefficient and *p*-value. The results show a positive correlation between DEF values and city size with a 95% confidence level. To better observe the difference in city size and imperviousness trend with DEF values, the imperviousness profiles of the cities are separated into three categories based on the rank order of DEF values, that is, small, medium, and large DEF, and averaged in each category (see Figure S9 in Supporting Information S1). It demonstrates the same trend that the smaller DEF values correspond to smaller city sizes.

Given the similar dominant wind directions among cities, the absolute wind direction of the west (W), southwest (SW), and south (S) directions are also analyzed as they include all the first dominant wind directions and

LU ET AL. 11 of 15



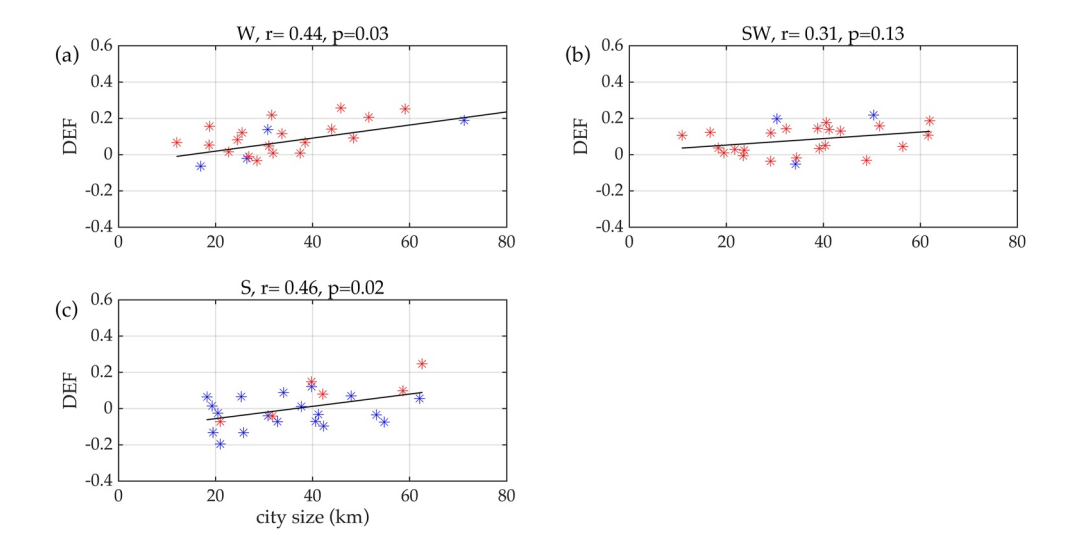


Figure 8. DEF versus city size for (a) W, (b) SW, and (c) S directions. Red markers in each subplot indicate city with that wind direction being the first or second dominant one.

the majority of the second dominant wind directions. Figure 8 shows that the DEF values tend to be positively correlated with city sizes for these wind directions, with the p-value being smaller than 0.15, while the other directions do not have obvious relationships with the p-value larger than 0.4 (see Figure S10 in Supporting Information S1).

To summarize, the DEF values are highly dependent on the wind direction, which could be related to different meteorological weather patterns and/or localized convective systems. The first two dominant wind directions of precipitating hours of those cities are analyzed and seen as air with similar properties. The wind rose shows consistency among cities, and the W and SW are the dominant wind direction for the majority of the cities. The influence of properties of the local urban forms, that is, imperviousness and city size, is then analyzed, and the results show that the city size is positively correlated with DEF values for these two directions.

4. Conclusion

In this study, we conduct a cross-city analysis using the Multi-Radar Multi-Sensor (MRMS) quantitative precipitation estimation data products for a selected set of cities across the continental United States from the years 2015–2021, considering a broad spectrum of urban forms and regional settings. The research goal is to unravel how different urban forms impact the spatial patterns of precipitation climatology under different meteorological conditions. The analysis focuses on the statistical performance rather than tracking the development of a single storm event. A few key takeaway points are summarized here:

- 1. The downwind enhancement of precipitation does exist for the majority of the study areas at the climatological time scale. The center of the precipitation is located at approximately 20–40 km downwind direction from the city center, which is consistent with previous studies (e.g., J. Liu & Niyogi, 2019; Lorenz et al., 2019).
- 2. The precipitation spatial pattern shows different characteristics with varying precipitation intensities, which have consistency across the cities. For higher-intensity precipitating hours, the spatial pattern is more clustered, and the precipitation center is closer to the city center in the downwind region. For lower-intensity precipitating hours, the precipitation is more intense around the city.
- 3. The DEF values do not show a clear trend with background wind speed, while the interaction between urban form and wind speeds does change and shows variable spatial patterns indicated by the 1D and 2D metrics. Specifically, the precipitation spatial pattern tends to be more scattered for lower wind speeds. In addition, the location for precipitation maxima tends to be closer to the city center under lower wind speeds due to the combined impacts induced by local urban-rural circulation and regional background wind.
- 4. Due to the inherent limitations of observational data to quantify the causal effects of different urban forms on the resulting precipitation pattern, this study is framed to understand the background meteorological condition

LU ET AL. 12 of 15

23284277, 2024, 1, Downloaded from

Wiley Online Library on [07/02/2024]. See the Term

under which a generalizable relationship between the urban form (in this case the city size) and downwind precipitation enhancement emerges. We find that DEF values are highly dependent on wind direction and have a positive relationship with city sizes for the first and second dominant wind directions. This implies that the mesoscale meteorological factor (i.e., wind direction) and the local factor (i.e., the urban form) synergistically affect the spatial pattern of precipitation climatology. It can be hypothesized based on observational evidence that cities growing bigger in size might experience higher downwind precipitation enhancement. We expect that controlled modeling studies in the future will be helpful to test the hypothesis and better understand the mechanisms.

Results of this study imply that some generalizable insight into precipitation pattern in urban areas can be gained by considering mesoscale meteorological conditions, urban form, and their interactions. This implies that it is important for studies aimed at understanding and reducing future urban hydroclimatic risks to investigate the mechanistic contribution of urban form, such as city size and spatial distribution of urban areas relative to the climatological dominant wind directions. One caveat of this study is to limit the analysis of precipitation pattern to downwind enhancement and the location of the radial precipitation maximum. This overlooks the documented lateral enhancement of precipitation that can be caused by the storm bifurcation (Bornstein & Lin, 2000; J. Liu & Niyogi, 2019). Another limitation is that the effect of aerosols on precipitation patterns is not considered, as we focus on the regional meteorological and local urban form factors that are directly relevant to the thermal and roughness effects of urban modification of precipitation. Future observational studies might address both caveats by defining different metrics for precipitation pattern and a more in-depth analysis of the spatial distribution of aerosols (Schmid & Niyogi, 2017).

Data Availability Statement

The MRMS data used in this study is available from NOAA National Severe Storms Laboratory data sets (NOAA/National Severe Storms Laboratory (NSSL), 2022). The MERRA-2 data can be obtained from Global Modeling and Assimilation Office and Pawson (2015). The MODIS land cover type product is obtained from Friedl and Sulla-Menashe (2022).

Acknowledgments

This work is funded by NASA's Interdisciplinary Research in Earth Science (IDS) program (80NSSC20K1263). QL acknowledges support from the US National Science Foundation (NSF-CA-REER-2143664, NSF-AGS-2028633, NSF-CBET-2028842) and computational resources from the National Center for Atmospheric Research (UCOR-0049) XC is supported by the U.S. Department of Energy Office of Science Biological and Environmental Research as part of the Regional and Global Model Analysis program area as part of the multiprogram Integrated Coastal Modeling (ICoM) project. The Pacific Northwest National Laboratory is operated for U.S. DOE by Battelle Memorial Institute under Contract DE-AC05-76RL01830.

References

- Andreae, M., & Rosenfeld, D. (2008). Aerosol–cloud–precipitation interactions. Part 1. The nature and sources of cloud-active aerosols. Earth-Science Reviews, 89(1), 13–41. https://doi.org/10.1016/j.earscirev.2008.03.001
- Booth, R. K., Kutzbach, J. E., Hotchkiss, S. C., & Bryson, R. A. (2006). A reanalysis of the relationship between strong westerlies and precipitation in the Great Plains and Midwest regions of North America. *Climatic Change*, 76(3–4), 427–441. https://doi.org/10.1007/s10584-005-9004-3
 Bornstein, R., & Lin, Q. (2000). Urban heat islands and summertime convective thunderstorms in Atlanta: Three case studies. *Atmospheric Environment*, 34(3), 507–516. https://doi.org/10.1016/S1352-2310(99)00374-X
- Cotton, W. R., & Pielke, R. A. (2007). Urban-induced changes in precipitation and weather. In *Human impacts on weather and climate* (2nd ed., pp. 90–101). Cambridge University Press. https://doi.org/10.1017/CBO9780511808319.007
- Dou, J., Wang, Y., Bornstein, R., & Miao, S. (2015). Observed spatial characteristics of Beijing urban climate impacts on summer thunderstorms. Journal of Applied Meteorology and Climatology, 54(1), 94–105. https://doi.org/10.1175/JAMC-D-13-0355.1
- Freitag, B. M., Nair, U. S., & Niyogi, D. (2018). Urban modification of convection and rainfall in complex terrain. *Geophysical Research Letters*, 45(5), 2507–2515. https://doi.org/10.1002/2017GL076834
- Friedl, M., McIver, D., Hodges, J., Zhang, X., Muchoney, D., Strahler, A., et al. (2002). Global land cover mapping from MODIS: Algorithms and early results. *Remote Sensing of Environment*, 83(1), 287–302. (The Moderate Resolution Imaging Spectroradiometer (MODIS): a new generation of Land Surface Monitoring). https://doi.org/10.1016/S0034-4257(02)00078-0
- Friedl, M., & Sulla-Menashe, D. (2022). MODIS/Terra+Aqua land cover type yearly L3 global 500m SIN grid V061 [Dataset]. NASA EOSDIS Land Processes Distributed Active Archive Center. https://doi.org/10.5067/MODIS/MCD12Q1.061
- Friedl, M., Sulla-Menashe, D., Tan, B., Schneider, A., Ramankutty, N., Sibley, A., & Huang, X. (2010). Modis collection 5 global land cover: Algorithm refinements and characterization of new datasets. *Remote Sensing of Environment*, 114(1), 168–182. https://doi.org/10.1016/j.
- Ganeshan, M., Murtugudde, R., & Imhoff, M. L. (2013). A multi-city analysis of the UHI-influence on warm season rainfall. *Urban Climate*, 6, 1–23. https://doi.org/10.1016/j.uclim.2013.09.004
- Gelaro, R., McCarty, W., Suárez, M. J., Todling, R., Molod, A., Takacs, L., et al. (2017). The Modern-Era Retrospective Analysis for Research and Applications, version 2 (MERRA-2). *Journal of Climate*, 30(14), 5419–5454. https://doi.org/10.1175/JCLI-D-16-0758.1
- Global Modeling and Assimilation Office, & Pawson, S. (2015). MERRA-2 tavg1_2d_slv_nx: 2d, 1-hourly, time-averaged, single-level, assimilation, single-level diagnostics V5.12.4 [Dataset]. NASA Goddard Earth Sciences Data and Information Services Center. https://doi.org/10.5067/VJAFPL11CSIV
- Han, J. Y., Baik, J. J., & Lee, H. (2014). Urban impacts on precipitation. Asia-Pacific Journal of Atmospheric Sciences, 50(1), 17–30. https://doi.org/10.1007/s13143-014-0016-7
- Hansen, M. C., Defries, R. S., Townshend, J. R. G., & Sohlberg, R. (2000). Global land cover classification at 1 km spatial resolution using a classification tree approach. *International Journal of Remote Sensing*, 21(6–7), 1331–1364. https://doi.org/10.1080/014311600210209

LU ET AL. 13 of 15

23284277, 2024, 1, Downloaded from

- Huff, F. A. (1975). Urban effects on the distribution of heavy convective rainfall. Water Resources Research, 11(6), 889–896. https://doi.org/10.1029/WR011i006p00889
- Huff, F. A., & Changnon, S. A. (1973). Precipitation modification by major urban areas. *Bulletin of the American Meteorological Society*, 54(12), 1220–1233. https://doi.org/10.1175/1520-0477(1973)054(1220:PMBMUA)2.0.CO;2
- Katz, R. W., Parlange, M. B., & Tebaldi, C. (2003). Stochastic modeling of the effects of large-scale circulation on daily weather in the southeastern U.S. In L. O. Mearns (Ed.), Issues in the impacts of climate variability and change on agriculture: Applications to the southeastern United States (pp. 189–216). Springer Netherlands. https://doi.org/10.1007/978-94-017-1984-1_9
- Kellner, O., & Niyogi, D. (2014). Land surface heterogeneity signature in tornado climatology? An illustrative analysis over Indiana, 1950–2012. Earth Interactions, 18(10), 1–32. https://doi.org/10.1175/2013EI000548.1
- Kingfield, D. M., Calhoun, K. M., de Beurs, K. M., & Henebry, G. M. (2018). Effects of city size on thunderstorm evolution revealed through a multiradar climatology of the central United States. *Journal of Applied Meteorology and Climatology*, 57(2), 295–317. https://doi.org/10.1175/ JAMC-D-16-0341.1
- Lehning, M., Löwe, H., Ryser, M., & Raderschall, N. (2008). Inhomogeneous precipitation distribution and snow transport in steep terrain. Water Resources Research, 44(7). https://doi.org/10.1029/2007wr006545
- Lengfeld, K., Kirstetter, P.-E., Fowler, H. J., Yu, J., Becker, A., Flamig, Z., & Gourley, J. (2020). Use of radar data for characterizing extreme precipitation at fine scales and short durations. *Environmental Research Letters*, 15(8), 085003. https://doi.org/10.1088/1748-9326/ab98b4
- Levin, Z., & Cotton, W.R. (2009). Aerosol pollution impact on precipitation: A scientific review. Springer. https://doi.org/10.1007/978-1-4020-8690-8
 Li, W., Li, L., Fu, R., Deng, Y., & Wang, H. (2011). Changes to the North Atlantic subtropical high and its role in the intensification of summer rainfall variability in the southeastern United States. Journal of Climate, 24(5), 1499–1506. https://doi.org/10.1175/2010JCL13829.1
- Liu, J., & Niyogi, D. (2019). Meta-analysis of urbanization impact on rainfall modification. Scientific Reports, 9(1), 7301. https://doi.org/10.1038/s41598-019-42494-2
- Liu, Y.-Y., Li, L., Liu, Y.-S., Chan, P.-W., Zhang, W.-H., & Zhang, L. (2021). Estimation of precipitation induced by tropical cyclones based on machine-learning-enhanced analogue identification of numerical prediction. *Meteorological Applications*, 28(2), e1978. https://doi. org/10.1002/met.1978
- Lorenz, J. M., Kronenberg, R., Bernhofer, C., & Niyogi, D. (2019). Urban rainfall modification: Observational climatology over Berlin, Germany. Journal of Geophysical Research: Atmospheres, 124(2), 731–746. https://doi.org/10.1029/2018JD028858
- McCarty, W., Coy, L., Gelaro, R., Huang, A., Merkova, D., Smith, E. B., et al. (2016). MERRA-2 input observations: Summary and assessment. Technical report series on global modeling and data assimilation (Vol. 46). Retrieved from https://ntrs.nasa.gov/citations/20160014544
- Miao, S., Chen, F., Li, Q., & Fan, S. (2011). Impacts of urban processes and urbanization on summer precipitation: A case study of heavy rainfall in Beijing on 1 august 2006. Journal of Applied Meteorology and Climatology, 50(4), 806–825. https://doi.org/10.1175/2010JAMC2513.1
- National Research Council. (2012). *Urban meteorology: Forecasting, monitoring, and meeting users' needs*. The National Academies Press. https://doi.org/10.17226/13328
- Ngarambe, J., Oh, J. W., Su, M. A., Santamouris, M., & Yun, G. Y. (2021). Influences of wind speed, sky conditions, land use and land cover characteristics on the magnitude of the urban heat island in Seoul: An exploratory analysis. Sustainable Cities and Society, 71, 102953. https:// doi.org/10.1016/j.scs.2021.102953
- NOAA/National Severe Storms Laboratory (NSSL). (2022). Multi-radar/multi-sensor (MRMS) precipitation data [Dataset]. NOAA/National Severe Storms Laboratory (NSSL). Retrieved from https://www.nssl.noaa.gov/projects/mrms/
- Oke, T. R. (1982). The energetic basis of the urban heat island. Quarterly Journal of the Royal Meteorological Society, 108(455), 1–24. https://doi.org/10.1002/gi.49710845502
- Omidvar, H., Bou-Zeid, E., Li, Q., Mellado, J.-P., & Klein, P. (2020). Plume or bubble? Mixed-convection flow regimes and city-scale circulations. *Journal of Fluid Mechanics*, 897, A5. https://doi.org/10.1017/jfm.2020.360
- Pathirana, A., Denekew, H. B., Veerbeek, W., Zevenbergen, C., & Banda, A. T. (2014). Impact of urban growth-driven landuse change on micro-climate and extreme precipitation—A sensitivity study. Atmospheric Research, 138, 59–72. https://doi.org/10.1016/j.atmosres.2013.10.005
- Santamouris, M. (2015). Analyzing the heat island magnitude and characteristics in one hundred Asian and Australian cities and regions. Science of the Total Environment, 512–513, 582–598. https://doi.org/10.1016/j.scitotenv.2015.01.060
- Schmid, P. E., & Niyogi, D. (2017). Modeling urban precipitation modification by spatially heterogeneous aerosols. *Journal of Applied Meteorology and Climatology*, 56(8), 2141–2153. https://doi.org/10.1175/JAMC-D-16-0320.1
- Seino, N., Aoyagi, T., & Tsuguti, H. (2018). Numerical simulation of urban impact on precipitation in Tokyo: How does urban temperature rise affect precipitation? *Urban Climate*, 23, 8–35. (ICUC9: The 9th International Conference on Urban Climate). https://doi.org/10.1016/j. uclim.2016.11.007
- Shem, W., & Shepherd, M. (2009). On the impact of urbanization on summertime thunderstorms in Atlanta: Two numerical model case studies. Atmospheric Research, 92(2), 172–189. https://doi.org/10.1016/j.atmosres.2008.09.013
- Shen, Y., & Yang, L. (2023). Divergent urban signatures in rainfall anomalies explained by pre-storm environment contrast. Geophysical Research Letters, 50(5), e2022GL101658. https://doi.org/10.1029/2022GL101658
- Shepherd, J., Stallins, J., Jin, M., & Mote, T. (2010). Urbanization: Impacts on clouds, precipitation, and lightning. In *Urban ecosystem ecology* (pp. 1–28). John Wiley Sons, Ltd. https://doi.org/10.2134/agronmonogr55.c1
- Shepherd, J. M. (2005). A review of current investigations of urban-induced rainfall and recommendations for the future. *Earth Interactions*, 9(12), 1–27. https://doi.org/10.1175/EI156.1
- Shepherd, J. M., Pierce, H., & Negri, A. J. (2002). Rainfall modification by major urban areas: Observations from spaceborne rain radar on the TRMM satellite. *Journal of Applied Meteorology and Climatology*, 41(7), 689–701. https://doi.org/10.1175/1520-0450(2002)041<0689:rmbmua>2.0.co;2
- Simón-Moral, A., Dipankar, A., Doan, Q.-V., Sanchez, C., Roth, M., Becker, E., & Huang, X.-Y. (2021). Urban intensification of convective rainfall over the Singapore—Johor Bahru region. *Quarterly Journal of the Royal Meteorological Society*, 147(740), 3665–3680. https://doi.org/10.1002/gi.4147
- Sungmin, O., & Kirstetter, P.-E. (2018). Evaluation of diurnal variation of GPM IMERG-derived summer precipitation over the contiguous US using MRMS data. *Quarterly Journal of the Royal Meteorological Society*, 144(S1), 270–281. https://doi.org/10.1002/qj.3218
- Tang, L., Zhang, J., Simpson, M., Arthur, A., Grams, H., Wang, Y., & Langston, C. (2020). Updates on the radar data quality control in the MRMS quantitative precipitation estimation system. *Journal of Atmospheric and Oceanic Technology*, 37(9), 1521–1537. https://doi.org/10.1175/
- Tao, W.-K., Li, X., Khain, A., Matsui, T., Lang, S., & Simpson, J. (2007). Role of atmospheric aerosol concentration on deep convective precipitation: Cloud-resolving model simulations. *Journal of Geophysical Research*, 112(D24), D24S18. https://doi.org/10.1029/2007JD008728

LU ET AL. 14 of 15

23284277, 2024, 1, Downloaded from https

doi/10.1029/2023EF003846 by Cochrane Luxembourg, Wiley Online Library on [07/02/2024]. See the Terms and Conditions (https://onlinelibrary.wiley.com/term

and-conditions) on Wiley Online Library for rules of use; OA articles are governed by the applicable Creative

- Thielen, J., Wobrock, W., Gadian, A., Mestayer, P., & Creutin, J.-D. (2000). The possible influence of urban surfaces on rainfall development: A sensitivity study in 2D in the meso-γ-scale. *Atmospheric Research*, 54(1), 15–39. https://doi.org/10.1016/S0169-8095(00)00041-7
- United Nations. (2018). World urbanization prospects: The 2018 revision. Department of Economic and Social Affairs, Population Division. Yang, L., Li, Q., Yuan, H., Niu, Z., & Wang, L. (2021). Impacts of urban canopy on two convective storms with contrasting synoptic conditions
- over Nanjing, China. Journal of Geophysical Research: Atmospheres, 126(9), e2020JD034509. https://doi.org/10.1029/2020JD034509
 Yang, L., Smith, J., & Niyogi, D. (2019). Urban impacts on extreme monsoon rainfall and flooding in complex terrain. Geophysical Research
- Letters, 46(11), 5918–5927. https://doi.org/10.1029/2019gl083363

 Zhang, J., Howard, K., Langston, C., Kaney, B., Qi, Y., Tang, L., et al. (2016). Multi-radar multi-sensor (MRMS) quantitative precipitation estimation: Initial operating capabilities. Bulletin of the American Meteorological Society, 97(4), 621–638. https://doi.org/10.1175/BAMS-D-14-00174.1
- Zhang, W., Yang, J., Yang, L., & Niyogi, D. (2022). Impacts of city shape on rainfall in inland and coastal environments. *Earth's Future*, 10(5), e2022EF002654. https://doi.org/10.1029/2022EF002654
- Zhou, R., Rybski, D., & Kropp, J. P. (2017). The role of city size and urban form in the surface urban heat island. *Scientific Reports*, 7(1), 4791. https://doi.org/10.1038/s41598-017-04242-2

LU ET AL. 15 of 15